
Adaptive Kernel Density Estimation with Pre-training

Ruitong Zhang

Department of Statistics and Data Science
Tsinghua University
Beijing, China
zrt25@mails.tsinghua.edu.cn

Ke Deng*

Department of Statistics and Data Science
Tsinghua University
Beijing, China
kdeng@tsinghua.edu.cn

Abstract

Density estimation in high-dimensional settings is an important and challenging statistical problem. Traditional methods based on kernel smoothing are inefficient in high dimensions due to the difficulties in specifying appropriate location-adaptive kernels. In this work, we introduce pre-training, a key idea behind many cutting-edge AI technologies, to the context of non-parametric density estimation. By establishing a pre-trained neural network that can recommend an appropriate location-adaptive kernel for each sample point, efficient density estimation with adaptive kernels is achieved in high dimensions. A wide range of numerical experiments show that this strategy is highly effective for improving density-estimation accuracy, when the target distribution is close to the distribution family for pre-training. When the target distribution is substantially different from the pre-training distribution family, the benefit from the proposed pre-training strategy may be diluted, but can be reactivated by an additional fine-tuning procedure.

1 Introduction

Nonparametric density estimation is a fundamental problem in statistics and machine learning. Given n i.i.d. samples $X_{1:n} = (X_1, \dots, X_n)$ from a continuous target distribution F_0 on \mathbb{R}^d , the goal is to estimate f_0 , the density function of F_0 , in a non-parametric fashion. In the statistical literature, a rich collection of methods have been proposed for this important problem, including *kernel density estimation* (KDE) [Rosenblatt, 1956, Parzen, 1962] and smoothing splines [Wahba, 1990, Green and Silverman, 1994]. In parallel, modern machine learning has developed expressive neural density estimators, including autoregressive models [Germain et al., 2015, Papamakarios et al., 2017], normalizing flows [Dinh et al., 2017], and score-based generative models [Song et al., 2021]. Among these methods, KDE remains attractive in many applications, because it enjoys an explicit analytic form with easy evaluation and well-developed statistical theory [Silverman, 1986, Wand and Jones, 1994].

Like many other methods in this field, however, KDE typically suffers significant performance degradation due to the curse of dimensionality. When d , the dimensionality of the target distribution, is large, the geometry of f_0 is difficult to capture, and the kernel function controls not only the amount of smoothing, but also the orientation and anisotropy of the estimator [Wand and Jones, 1994, Chacón and Duong, 2018]. In these cases, using a common global kernel to smooth all regions of the sample space is often inadequate, especially when the target density has heterogeneous local scale or anisotropic geometry: sharp high-density regions may require narrow and directionally sensitive kernels, while sparse or diffuse regions may require flatter kernel functions.

Adaptive KDE methods [Terrell and Scott, 1992] mitigate this problem by allowing the bandwidth to vary across locations, with two common formulations being balloon estimators and sample-point

*Corresponding author.

estimators [Jones, 1990]. Existing adaptive KDE methods often construct these adaptive bandwidths from pilot density estimates [Abramson, 1982], nearest-neighbor distances [Breiman et al., 1977], or other local geometric information. Although statistically well motivated, these approaches typically adapt restricted kernel structures rather than learning a general rule to recommend appropriate location-adaptive kernels.

In this work, we fill this gap by introducing **pre-training**, a key idea behind many cutting-edge AI technologies, to the context of non-parametric density estimation. By establishing a pre-trained neural network ϕ_θ with θ as parameters that can recommend an appropriate location-adaptive kernel for each observed sample X_i based on its local geometry in $X_{1:n}$, we successfully resolve the problem of location-adaptive kernel specification that is often extremely difficult in the traditional learning framework with a limited number of samples. With the support of ϕ_θ , which encodes information learned during pre-training beyond the limited information contained in the observed sample $X_{1:n}$, efficient adaptive kernel density estimation can be achieved in relatively high-dimensional settings. To establish the pre-trained neural network ϕ_θ for kernel recommendation, we prepare a distribution family \mathcal{F} that covers a wide range of distributions of potential interest, and generate a large collection of synthetic data \mathcal{D} based on \mathcal{F} for pre-training of ϕ_θ .

Numerical experiments show that this *neural-network-guided KDE* (NNKDE) significantly outperforms existing KDE methods when the target distribution F_0 is close to \mathcal{F} . When F_0 is far away from \mathcal{F} , the advantage of NNKDE may be diluted, but it can be reactivated by an additional **fine-tuning** procedure, where the global scale of the recommended location-adaptive kernels can be further adjusted under the guidance of self-exclusive leave-one-out likelihood of $X_{1:n}$. Such a “pre-training + fine-tuning” strategy further enhances the adaptability of the proposed NNKDE, providing a powerful tool for non-parametric density estimation.

Our contributions are threefold. First, we formally introduce the idea of pre-training to non-parametric statistics and demonstrate its ability to improve the efficiency of statistical inference using synthetic data. Second, we show that the benefits of pre-training for non-parametric statistics can be further preserved and enhanced by an additional fine-tuning procedure, suggesting that the widely used “pre-training + fine-tuning” strategy may also be beneficial for statistical models. Third, we provide a systematic evaluation protocol to empirically compare different KDE methods in various settings.

2 Related Works

Bandwidth selection and adaptive KDE. Kernel density estimation has a long history in nonparametric statistics, with classical treatments covering both theoretical properties and practical bandwidth selection [Silverman, 1986, Wand and Jones, 1994]. In multivariate KDE, the bandwidth matrix is the central smoothing parameter, controlling scale, orientation, and anisotropy of the estimator [Wand and Jones, 1994, Chacón and Duong, 2018]. Classical bandwidth-selection rules include rule-of-thumb methods, plug-in selectors, and cross-validation-based criteria [Silverman, 1986, Sheather and Jones, 1991, Rudemo, 1982, Bowman, 1984]. Extensions to full bandwidth matrices have also been studied, including data-driven smooth cross-validation methods [Duong and Hazelton, 2005]. However, a single global bandwidth matrix can be inadequate for heterogeneous densities with spatially varying smoothness, and bandwidth optimization can be numerically unstable in multivariate settings [Hall and Marron, 1991]. Adaptive KDE methods address this limitation by allowing the bandwidth to vary locally. Classical examples include balloon estimators [Loftsgaarden and Quesenberry, 1965] and sample-point estimators [Breiman et al., 1977, Sain, 2002]. The latter are particularly relevant here because, under standard constructions, they retain a properly normalized density form [Terrell and Scott, 1992]. Existing adaptive methods often rely on pilot estimates or scalar local rescaling rules, such as Abramson’s square-root law [Abramson, 1982, Terrell and Scott, 1992]. In contrast, our work learns observation-specific positive definite bandwidth matrices within an explicit sample-point KDE.

Neural density estimation. A separate line of work uses neural networks to construct expressive density estimators. Autoregressive density estimators such as Masked Autoencoder for Distribution Estimation (MADE) model the joint density through conditional factorizations [Germain et al., 2015]. Normalizing flows, including Real-valued Non-Volume Preserving transformations (Real NVP) [Dinh et al., 2017] and masked autoregressive flow (MAF) [Papamakarios et al., 2017], learn

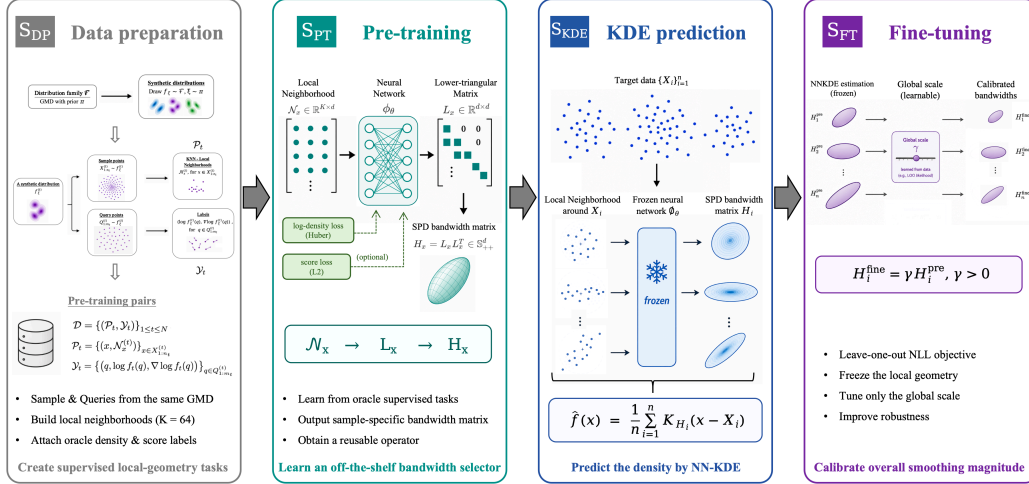


Figure 1: Workflow of NNKDE composed of four stages.

invertible transformations from simple base distributions to complex target distributions. Score-based generative models learn the score function and generate samples through stochastic dynamics [Song et al., 2021]. Other neural approaches have been developed for high-dimensional density estimation using deep generative models [Liu et al., 2021]. These approaches rely on neural approximation, but they primarily target direct density, score, or generative-map estimation. NNKDE differs in that the neural component is embedded inside an explicit KDE estimator rather than replacing the estimator itself.

Amortized and pre-trained density learning. The pre-training strategy in this paper is related to amortized inference, where computation is shared across a family of related inference problems rather than repeated from scratch for each new instance [Gershman and Goodman, 2014]. A similar perspective appears in simulation-based inference, where simulation and surrogate learning are performed offline and then reused for new observations [Cranmer et al., 2020]. Related ideas have also been explored in density estimation, including data-driven density estimators trained over synthetic distribution families [Puchert et al., 2021], meta-learned conditional density estimators across related tasks [Ton et al., 2021], and transformer-based plug-in estimators for density and score estimation [Ilin and Sushko, 2026]. These approaches amortize density or score estimation directly. In contrast, NNKDE amortizes the bandwidth-selection rule inside a classical sample-point KDE, so pre-training is used to learn a transferable bandwidth functional rather than to replace the nonparametric estimator.

3 Method

In this work, we consider the following sample-point adaptive KDE for the target distribution F_0 based on i.i.d. samples $X_{1:n} \sim F_0$:

$$\hat{f}_{\text{SP}}(x | X_{1:n}) = \frac{1}{n} \sum_{i=1}^n K_{H_i}(x - X_i) \quad \forall x \in \mathbb{R}^d, \quad (1)$$

where H_i is a $d \times d$ covariance matrix (referred to as the bandwidth matrix hereinafter) associated with the sample point X_i , and $K_H(z) = |H|^{-1/2} \kappa(H^{-1/2}z)$ with κ being the d -dimensional standard Gaussian kernel. The bandwidth matrix H_i fully controls the geometric shape of the location-adaptive kernel associated with X_i . The proposed NNKDE relies on a pre-trained neural network ϕ_θ to recommend H_i for X_i . Figure 1 demonstrates the workflow of NNKDE, which is composed of four stages: the data preparation stage \mathcal{S}_{DP} , the pre-training stage \mathcal{S}_{PT} , the KDE stage \mathcal{S}_{KDE} , and the fine-tuning stage \mathcal{S}_{FT} . Next, we will introduce these four stages in sequence.

3.1 The pre-training data preparation stage \mathcal{S}_{DP}

This stage concerns preparation of the distribution family \mathcal{F} and the synthetic data \mathcal{D} defined in the Introduction for pre-training of ϕ_θ . Here, we specify \mathcal{F} as a family of *Gaussian mixture distributions* (GMDs), i.e., $\mathcal{F} = \{\text{GMD}_\xi\}_{\xi \sim \pi}$, due to their ease of operation and flexibility in distribution approximation, where GMD parameter ξ is randomly generated from a prior distribution π over the parameter space Ξ . In practice, we randomly generate N GMDs from \mathcal{F} , namely $\{F_t\}_{1 \leq t \leq N}$, where $F_t = \text{GMD}_{\xi_t}$ with $\xi_t \sim \pi$. Concrete specifications of Ξ and π are detailed in Appendix A, which ensures the rich diversity of \mathcal{F} .

For each obtained F_t , we draw a sample set $X_{1:n_t}^{(t)} \sim F_t$ together with an independent query set $Q_{1:m_t}^{(t)} \sim F_t$, leading to the following triplets $\{(F_t, X_{1:n_t}^{(t)}, Q_{1:m_t}^{(t)})\}_{1 \leq t \leq N}$. For each sample point $x \in X_{1:n_t}^{(t)}$, let $\mathcal{N}_x^{(t)}$ denote the $K \times d$ coordinate matrix of the K nearest neighbors of x in $X_{1:n_t}^{(t)}$ after a translation transformation of the sample space that moves x to the origin. The matrix $\mathcal{N}_x^{(t)}$ encodes the local geometric pattern around x in contrast to the background $X_{1:n_t}^{(t)}$, and

$$\mathcal{P}_t = \{(x, \mathcal{N}_x^{(t)})\}_{x \in X_{1:n_t}^{(t)}} \quad (2)$$

summarizes all local patterns of $X_{1:n_t}^{(t)}$. For each query point $q \in Q_{1:m_t}^{(t)}$, let $\log f_t(q)$ and $\nabla \log f_t(q)$ be logarithmic density and score of F_t at q , respectively. The collection of triplets

$$\mathcal{Y}_t = \{(q, \log f_t(q), \nabla \log f_t(q))\}_{q \in Q_{1:m_t}^{(t)}} \quad (3)$$

summarizes all order-0 and order-1 information about f_t , the density function of F_t , at $Q_{1:m_t}^{(t)}$. Pairing \mathcal{P}_t and \mathcal{Y}_t for each t , we obtain the following data set for the pre-training of ϕ_θ :

$$\mathcal{D} = \{(\mathcal{P}_t, \mathcal{Y}_t)\}_{1 \leq t \leq N}, \quad (4)$$

where \mathcal{Y}_t serves as the training guidance for input \mathcal{P}_t . In this study, we generated a huge pre-training data set via these steps by specifying $N = 500,000$, and $n_t = 2048$ and $m_t = 1024$ for all t .

3.2 The pre-training stage \mathcal{S}_{PT}

This stage concerns learning the neural kernel recommender ϕ_θ , whose architecture is detailed in Appendix B, from the pre-training data set \mathcal{D} prepared in the previous stage. For each element $(\mathcal{P}_t, \mathcal{Y}_t)$ in \mathcal{D} , neural network ϕ_θ digests $\mathcal{N}_x^{(t)}$ and recommends a lower-triangular matrix L_x determined by θ for each $x \in X_{1:n_t}^{(t)}$, which leads to a bandwidth matrix $H_x = L_x L_x^T$. We denote this procedure by the notation $H_x = \phi_\theta(\mathcal{N}_x)$, with the note that H_x is a function of θ . According to (1), these location-adaptive bandwidth matrices induce the following estimator for the fully known f_t :

$$\widehat{f}_\theta(x | X_{1:n_t}^{(t)}) = \frac{1}{n_t} \sum_{l=1}^{n_t} K_{H_l^{(t)}}(x - X_l^{(t)}) \quad \text{with} \quad H_l^{(t)} = \phi_\theta(\mathcal{N}_{X_l^{(t)}}^{(t)}), \quad (5)$$

whose score function has the closed form below:

$$\nabla_x \log \widehat{f}_\theta(x | X_{1:n_t}^{(t)}) = \sum_{l=1}^{n_t} \omega_l(x) \left\{ [H_l^{(t)}]^{-1} (X_l^{(t)} - x) \right\}, \quad \omega_l(x) = \frac{K_{H_l^{(t)}}(x - X_l^{(t)})}{\sum_{r=1}^{n_t} K_{H_r^{(t)}}(x - X_r^{(t)})}.$$

Comparing \widehat{f}_θ with f_t at query points $Q_{1:m_t}^{(t)}$, we obtain the following loss function w.r.t. $(\mathcal{P}_t, \mathcal{Y}_t)$:

$$\begin{aligned} \mathcal{L}_t(\theta) &= \frac{1}{m_t} \sum_{j=1}^{m_t} \rho \left(\log \widehat{f}_\theta(Q_j^{(t)} | X_{1:n_t}^{(t)}) - \log f_t(Q_j^{(t)}) \right) \\ &\quad + \lambda_{\text{score}} \cdot \frac{1}{m_t} \sum_{j=1}^{m_t} \left\| \nabla \log \widehat{f}_\theta(Q_j^{(t)} | X_{1:n_t}^{(t)}) - \nabla \log f_t(Q_j^{(t)}) \right\|_2^2, \end{aligned} \quad (6)$$

where ρ is the Huber loss, $\|\cdot\|_2$ is the L_2 loss, and $\lambda_{\text{score}} \geq 0$ controls the strength of the second term. Intuitively, the first term in $\mathcal{L}_t(\theta)$ guides ϕ_θ to produce bandwidth matrices that yield accurate density values, while the score term provides additional supervision on the higher order geometry of f_t . To keep a proper balance between these two terms, we specify $\lambda_{\text{score}} = 10^{-2}$ in this study.

Assembling the hybrid loss from different elements in \mathcal{D} , we obtain the overall loss to guide the pre-training of ϕ_θ , based on which θ can be optimized by AdamW [Loshchilov and Hutter, 2019] under the default setting with learning rate and weight decay both specified as 10^{-4} . In practice, however, to avoid memory overflow, we follow the mini-batch strategy to update θ according to the assembled loss of $B = 500$ elements in \mathcal{D} each epoch. It takes 1,000 epochs to scan through the pre-training set \mathcal{D} with $N = 500,000$ elements.

For each dimension d , we pre-trained a separate model on a single NVIDIA Tesla V100-SXM2-32GB GPU. Pre-training took approximately 15 GPU-hours for each dimension up to $d = 10$, and approximately 19, 27, and 39 GPU-hours for $d = 20$, $d = 30$, and $d = 50$, respectively.

3.3 The KDE stage \mathcal{S}_{KDE}

Let $\hat{\theta}$ be the optimized parameter obtained in the pre-training stage. Neural network $\phi_{\hat{\theta}}$ offers an off-the-shelf bandwidth-selection rule in downstream applications. Given the target sample $X_{1:n} \sim F_0$, $\phi_{\hat{\theta}}$ recommends for each X_i in $X_{1:n}$ the following bandwidth matrix

$$H_i^{\text{pre}} = \phi_{\hat{\theta}}(\mathcal{N}_{X_i}), \quad i = 1, \dots, n, \quad (7)$$

where \mathcal{N}_x denotes the $K \times d$ coordinate matrix of the K nearest neighbors of x in $X_{1:n}$ after a translation transformation of the sample space that moves x to the origin. These bandwidth matrices lead to the following estimator for f_0 :

$$\hat{f}_{\text{pre}}(x | X_{1:n}) = \frac{1}{n} \sum_{i=1}^n K_{H_i^{\text{pre}}}(x - X_i), \quad \forall x \in \mathbb{R}^d. \quad (8)$$

No target-specific retraining of the neural network is performed in this stage.

3.4 The fine-tuning stage \mathcal{S}_{FT}

When the target distribution differs from the pre-training family, the global smoothing scale of the pre-trained bandwidth matrices may need adjustment. We therefore adopt a lightweight scale-calibration step as the ‘‘fine-tuning’’ for the pre-trained $\phi_{\hat{\theta}}$. For this purpose, we modify the bandwidth matrices recommended by $\phi_{\hat{\theta}}$ with a global scalar $\gamma > 0$ as below:

$$H_i^{\text{fine}} = \gamma H_i^{\text{pre}}, \quad i = 1, \dots, n. \quad (9)$$

The optimal γ is obtained by minimizing a self-exclusive leave-one-out negative log-likelihood on the target sample, i.e.,

$$\gamma^* = \arg \min_{\gamma > 0} \left\{ -\frac{1}{n} \sum_{i=1}^n \log \left[\frac{1}{n-1} \sum_{j \neq i} K_{\gamma H_j^{\text{pre}}}(X_i - X_j) \right] \right\}. \quad (10)$$

The self-exclusion form removes the direct contribution of the kernel centered at X_i , protecting γ from being driven toward degenerate undersmoothing. Plugging γ^* into (9), we obtain the fine-tuned bandwidth matrices to improve adaptive KDE. Hereinafter, we refer to the NNKDE without and with the fine-tuning stage as NNKDE_{pre} and NNKDE_{fine}, respectively.

4 Experiments

In this section, we compare the performance of the proposed methods, i.e., NNKDE_{pre} and NNKDE_{fine}, with a collection of representative KDE and adaptive KDE methods in the literature. For KDE methods, we select the famous Silverman’s rule [Silverman, 1986] and likelihood cross-validation (LCV) [Rudemo, 1982, Bowman, 1984] as comparison baselines; for adaptive KDE methods, we select Abramson’s method [Abramson, 1982, Terrell and Scott, 1992] and kNN local-scaling

KDE (kNN) [Loftsgaarden and Quesenberry, 1965, Breiman et al., 1977] as comparison baselines. Moreover, to evaluate the effect of pre-training in NNKDE, we also include NNKDE_{scratch}, a naive version of NNKDE where the parameter θ of the neural network ϕ_θ is randomly initialized without further training, in the comparison. More details about the implementation of these baseline methods are provided in Appendix C.

4.1 Experimental setup

To systematically compare the performance of different methods, we set up 4 scenarios in which the target distribution F_0 comes from 4 different distribution families, namely GMD _{\mathcal{F}} , GMD _{\mathcal{F}^+} , Banana and NoisyTorus. Figure 2 presents the typical scatter plots of the four scenarios when $d = 2$. In the first scenario GMD _{\mathcal{F}} , the target distribution F_0 is generated from $\mathcal{F} = \{\text{GMD}_\xi\}_{\xi \sim \pi}$, the distribution family used in the pre-training of ϕ_θ . In all the other 3 scenarios, the target distribution F_0 is generated from alternative distribution families that do not overlap with \mathcal{F} . More details about these scenarios are provided in Appendix D.

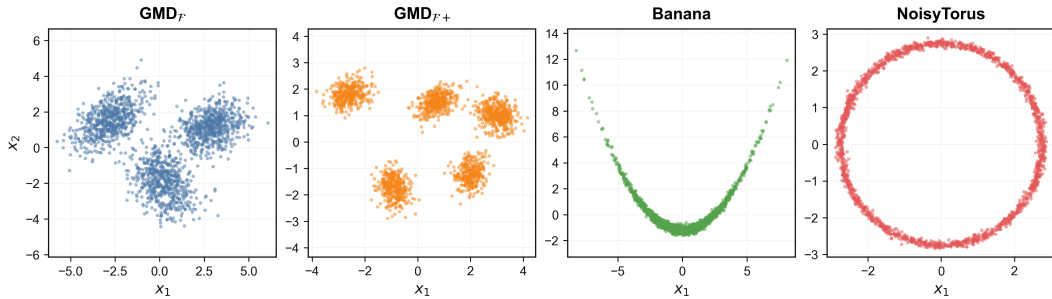


Figure 2: Representative two-dimensional samples from the four benchmark scenarios.

For each scenario, we choose the dimensionality $d \in \{2, 3, 5, 10, 30, 50\}$, and specify the sample size $n \in \{64, 256, 1024, 2048, 4096\}$ for low dimensional cases where $d \leq 5$, while $n \in \{2000, 5000, 10000, 15000, 20000\}$ for high dimensional cases where $d > 5$, resulting in $4 \times (3 \times 5 + 3 \times 5) = 120$ experimental settings.

For each experimental setting, we independently generate 10 target distribution instances. Within each target distribution instance, we draw 5 independent fitting samples and evaluate the resulting estimators on independent test sets sampled from the same distribution. This yields 50 runs for each experimental setting in total. We apply the 7 competing methods, namely Silverman, LCV, Abramson, kNN, NNKDE_{scratch}, NNKDE_{pre}, and NNKDE_{fine}, to all runs, and evaluate their performance by the normalized out-of-sample negative log-likelihood (NLL) defined below:

$$\text{NLL}(\hat{f}) = -\frac{1}{N_{\text{eva}}} \sum_{j=1}^{N_{\text{eva}}} \log \hat{f}(Z_j)/d, \quad (11)$$

where \hat{f} denotes the density estimator obtained from a specific method, and $\{Z_j\}_{j=1}^{N_{\text{eva}}}$ is an independent test set sampled from the corresponding target distribution instance. We set $N_{\text{eva}} = 3000$ in all experiments. A smaller NLL indicates better out-of-sample likelihood performance, and normalization by the ambient dimension d facilitates comparison across dimensions. For each experimental setting, we report the mean and standard deviation across the 10 target distribution instances after averaging over the 5 replicates within each instance.

Moreover, to better judge how the competing methods approach the theoretical optimal performance, we also evaluate the performance of the true density f_0 under the same evaluation protocol. We refer to this upper bound method as Oracle, which helps highlight the performance gap between NNKDE and theoretical optimum.

4.2 Results

Figure 3 compares the performance of different methods in terms of average NLL in 4 evaluation scenarios with different combinations of d and n . From the figure, we observe the following patterns.

First, $\text{NNKDE}_{\text{fine}}$ uniformly outperforms all competing methods in almost all experimental settings, indicating that the proposed “pre-training + fine-tuning” framework is a promising solution to the challenging problem of adaptive KDE. Second, $\text{NNKDE}_{\text{fine}}$ quickly approaches Oracle in most low-dimensional settings, but maintains an obvious distance to Oracle in most high-dimensional cases, suggesting that more efforts are needed along this research line for more efficient adaptive KDE in high dimensions. Third, $\text{NNKDE}_{\text{pre}}$ yields competitive performance in scenarios $\text{GMD}_{\mathcal{F}}$ and $\text{GMD}_{\mathcal{F}+}$ (almost identical to $\text{NNKDE}_{\text{fine}}$ in scenarios $\text{GMD}_{\mathcal{F}}$ as expected) and obvious performance degradation in scenarios Banana and NoisyTorus, confirming that the fine-tuning stage is critical to the success of $\text{NNKDE}_{\text{fine}}$. Fourth, $\text{NNKDE}_{\text{scratch}}$ performs poorly in most cases, revealing the important role of the pre-training stage in the proposed methods.

Moreover, Table A1 provides additional comparison of different methods in the cross-section of $n = 4,096$ with more numerical details. Each cell in the table reports two numbers for an experimental setting: the average NLL and the corresponding standard deviation. In general, the table delivers similar messages as in Figure 3. An interesting discovery from this table is that the NNKDE methods tend to enjoy a smaller performance variation than the other methods in most high-dimensional cases. Together with the results in Figure 3, these findings demonstrate the potential of NNKDE as a framework that integrates neural networks with statistical inference through pre-training and fine-tuning.

5 Conclusions and Discussions

We proposed NNKDE , a sample-point adaptive KDE method that adopts reusable kernel selection rules encoded in a pre-trained neural network, while preserving the explicit KDE form. Systematic numerical experiments confirm the effectiveness of the proposed method in improving the accuracy of non-parametric density estimation, and the critical role of the pre-training and fine-tuning stages built in the approach. These results suggest a promising way to bring amortized pre-training into adaptive nonparametric density estimation and beyond, which may reshape many areas of non-parametric statistics.

Although the pre-training stage of NNKDE is computationally very expensive, once the pre-training is finished, applying NNKDE in practice is computationally convenient. This paradigm of heavy offline computing but light online computing keeps a perfect balance between pursuit of excellent performance and saving data and computing resources. This property grants NNKDE great advantages in practical applications with a limited computation budget.

Unlike other neural KDE methods, which directly approximate the unknown density function via a neural network, NNKDE utilizes a neural network to learn a more fundamental bandwidth selection rule from local geometric properties of the distribution family for pre-training in advance, which can be further adjusted via fine-tuning after the real task is received. Such a pipeline is an exact analogy to the “pre-training + fine-tuning” framework which has been widely adopted in image and natural language processing. On the other hand, because NNKDE takes KDE as the primary framework to integrate a pre-trained neural network, it retains the transparency and interpretability typically associated with statistical models but often absent from deep learning models.

Despite the many advantages mentioned above, the NNKDE introduced in this paper still has many limitations. First, the pre-training dataset is limited to Gaussian mixtures with only a few Gaussian components, greatly restricting the pre-training module from releasing greater power. Second, the current architecture of the neural kernel recommender ϕ_{θ} is not flexible enough to support a varying ambient dimension d . Such a limitation makes it inefficient to utilize cross-dimensional pre-training information and deal with degenerate distributions, e.g., those in the NoisyTorus scenario, whose probability mass is concentrated near a lower-dimensional manifold of the space. Third, the current fine-tuning strategy to adjust a single global scalar factor is too naive to meet the heterogeneous fine-tuning demand in different local regions of the target family. More flexible fine-tuning mechanisms need to be investigated to further improve effectiveness and adaptability of pre-training.

NNKDE utilizes synthetic data heavily in its pre-training stage. However, unlike most recent work that constructs synthetic data for model training, NNKDE uses synthetic data for pre-training instead. This new paradigm of using synthetic data introduces many new perspectives and problems regarding the construction and utilization of synthetic data. When synthetic data are used for model training, they are often interpreted as an informal prior from a Bayesian perspective, and their impact

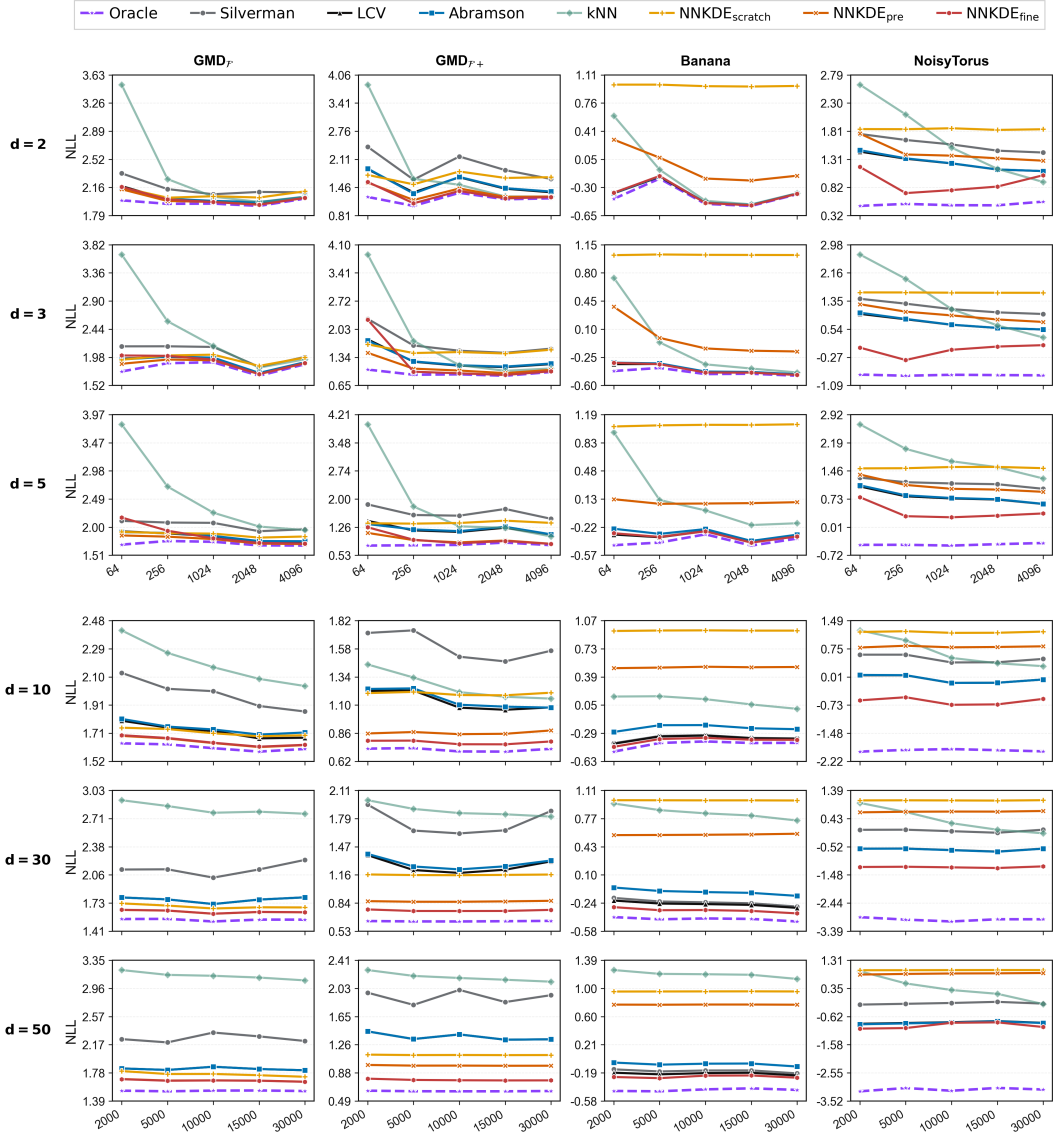


Figure 3: Performance of different methods in terms of normalized negative log-likelihood.

on statistical inference is studied under distributional drift between real and synthetic data. When synthetic data are used for pre-training followed by fine-tuning, a new framework is needed because the role of synthetic data becomes more subtle.

As a new effort to integrate deep learning and statistical learning for more efficient data analysis, NNKDE is unique in its initiative to enhance a complex neural network with pre-training. Embedding a complex neural network without sufficient pre-training into a statistical model is often dangerous in practice because the limited sample size in a typical statistical problem usually makes it unaffordable to drive the expensive neural network. In these cases, establishing a wise framework to effectively utilize the rich information in a well pre-trained neural network indirectly, just as what NNKDE achieves, is often an attractive choice.

6 Acknowledgments

The authors thank colleagues and seminar participants for helpful discussions and constructive feedback. Any remaining errors are our own.

References

- Ian S. Abramson. On bandwidth variation in kernel estimates—a square root law. *The Annals of Statistics*, 10(4):1217–1223, 1982.
- Adrian W. Bowman. An alternative method of cross-validation for the smoothing of density estimates. *Biometrika*, 71(2):353–360, 1984.
- Leo Breiman, William Meisel, and Edward Purcell. Variable kernel estimates of multivariate densities. *Technometrics*, 19(2):135–144, 1977.
- José E. Chacón and Tarn Duong. *Multivariate Kernel Smoothing and Its Applications*. Chapman and Hall/CRC, 2018.
- Kyle Cranmer, Johann Brehmer, and Gilles Louppe. The frontier of simulation-based inference. *Proceedings of the National Academy of Sciences of the United States of America*, 117(48):30055–30062, 2020.
- Laurent Dinh, Jascha Sohl-Dickstein, and Samy Bengio. Density estimation using real NVP. In *International Conference on Learning Representations*, 2017.
- Tarn Duong and Martin L. Hazelton. Cross-validation bandwidth matrices for multivariate kernel density estimation. *Scandinavian Journal of Statistics*, 32(3):485–506, 2005.
- Mathieu Germain, Karol Gregor, Iain Murray, and Hugo Larochelle. Made: Masked autoencoder for distribution estimation. In *Proceedings of the 32nd International Conference on Machine Learning*, volume 37 of *Proceedings of Machine Learning Research*, pages 881–889. PMLR, 2015.
- Samuel J. Gershman and Noah D. Goodman. Amortized inference in probabilistic reasoning. In *Proceedings of the Annual Meeting of the Cognitive Science Society*, volume 36, pages 517–522, 2014.
- Peter J. Green and Bernard W. Silverman. *Nonparametric Regression and Generalized Linear Models: A Roughness Penalty Approach*. Chapman and Hall, 1994.
- Peter Hall and J. S. Marron. Local minima in cross-validation functions. *Journal of the Royal Statistical Society: Series B (Methodological)*, 53(1):245–252, 1991.
- Vasily Ilin and Peter Sushko. Discoformer: Plug-in density and score estimation with transformers, 2026.
- M. C. Jones. Variable kernel density estimates and variable kernel density estimates. *Australian Journal of Statistics*, 32(3):361–371, 1990.
- Qiao Liu, Jiaye Xu, Rui Jiang, and Wing Hung Wong. Density estimation using deep generative neural networks. *Proceedings of the National Academy of Sciences of the United States of America*, 118(15):e2101344118, 2021.
- D. O. Loftsgaarden and C. P. Quesenberry. A nonparametric estimate of a multivariate density function. *The Annals of Mathematical Statistics*, 36(3):1049–1051, 1965.
- Ilya Loshchilov and Frank Hutter. Decoupled weight decay regularization. In *International Conference on Learning Representations*, 2019.
- George Papamakarios, Theo Pavlakou, and Iain Murray. Masked autoregressive flow for density estimation. In *Advances in Neural Information Processing Systems 30*, pages 2338–2347, 2017.
- Emanuel Parzen. On estimation of a probability density function and mode. *The Annals of Mathematical Statistics*, 33(3):1065–1076, 1962.
- Patrik Puchert, Pedro Hermosilla, Tobias Ritschel, and Timo Ropinski. Data-driven deep density estimation. *Neural Computing and Applications*, 33:16773–16807, 2021.
- Murray Rosenblatt. Remarks on some nonparametric estimates of a density function. *The Annals of Mathematical Statistics*, 27(3):832–837, 1956.

- Mats Rudemo. Empirical choice of histograms and kernel density estimators. *Scandinavian Journal of Statistics*, 9(2):65–78, 1982.
- Stephan R. Sain. Multivariate locally adaptive density estimation. *Computational Statistics & Data Analysis*, 39(2):165–186, 2002.
- David W. Scott. *Multivariate Density Estimation: Theory, Practice, and Visualization*. Wiley, 1992.
- Simon J. Sheather and Michael C. Jones. A reliable data-based bandwidth selection method for kernel density estimation. *Journal of the Royal Statistical Society: Series B (Methodological)*, 53(3):683–690, 1991.
- Bernard W. Silverman. *Density Estimation for Statistics and Data Analysis*. Monographs on Statistics and Applied Probability. Chapman and Hall, 1986.
- Yang Song, Jascha Sohl-Dickstein, Diederik P. Kingma, Abhishek Kumar, Stefano Ermon, and Ben Poole. Score-based generative modeling through stochastic differential equations. In *International Conference on Learning Representations*, 2021.
- George R. Terrell and David W. Scott. Variable kernel density estimation. *The Annals of Statistics*, 20(3):1236–1265, 1992.
- Jean-Francois Ton, Lucian Chan, Yee Whye Teh, and Dino Sejdinovic. Noise contrastive meta-learning for conditional density estimation using kernel mean embeddings. In *Proceedings of The 24th International Conference on Artificial Intelligence and Statistics*, volume 130 of *Proceedings of Machine Learning Research*, pages 1099–1107. PMLR, 2021.
- Grace Wahba. *Spline Models for Observational Data*, volume 59 of *CBMS-NSF Regional Conference Series in Applied Mathematics*. SIAM, 1990.
- M. P. Wand and M. C. Jones. *Kernel Smoothing*. Monographs on Statistics and Applied Probability. Chapman and Hall, 1994.

A Details on Synthetic Pre-training Data Generation

Here, we provide concrete specification of the ‘‘prior’’ distribution π over Ξ , which defines $\mathcal{F} = \{\text{GMD}_\xi\}_{\xi \sim \pi}$, the family of Gaussian mixture distributions for the pre-training of ϕ_θ . For a GMD F_ξ from \mathcal{F} , its density is

$$f_\xi(x) = \sum_{k=1}^K w_k \mathcal{N}(x; \mu_k, \Sigma_k), \quad (\text{A1})$$

where $\xi = \{K, w_{1:K}, \mu_{1:K}, \Sigma_{1:K}\}$. We specify π as follows: the number of mixture components $K \sim \text{Unif}\{1, \dots, 8\}$, the weight vectors $w_{1:K} \sim \text{Dirichlet}(0.8 \times \mathbf{1}_K)$, the component means $\mu_k \sim \text{Unif}([-10, 10]^d)$, and the component covariance matrix Σ_k is generated by randomly sampling its eigenvalues from $\text{Unif}([0.25, 2.5])$ and specifying its eigenvectors with a random rotation matrix in \mathbb{R}^d .

B Architecture of the Neural Kernel Recommender ϕ_θ

To describe the architecture independently of its use inside KDE, we use $\eta \in \mathbb{R}^d$ to denote a generic reference location. Let

$$\mathcal{N}_\eta = \{r_\ell = u_\ell - \eta : u_\ell \in \text{kNN}(\eta)\}_{\ell=1}^{K_{\text{nn}}} \in \mathbb{R}^{K_{\text{nn}} \times d}. \quad (\text{A2})$$

The neural bandwidth recommender maps this local neighbourhood geometry to a symmetric positive definite bandwidth matrix,

$$\phi_\theta : \mathcal{N}_\eta \mapsto H_\eta. \quad (\text{A3})$$

Here η is only a generic reference location for describing the architecture. In pre-training, it is instantiated as a point in the fitting sample $X_{1:n_i}^{(i)}$; in the KDE stage, it is instantiated as a target sample point X_i .

Internally, the network uses an SPD-constrained output parameterization. Specifically, it outputs a lower-triangular factor L_η and sets

$$H_\eta = L_\eta L_\eta^\top. \quad (\text{A4})$$

This implementation detail ensures that the bandwidth matrix returned by ϕ_θ is positive definite, while the main text uses the simpler notation $\phi_\theta(\mathcal{N}_\eta) = H_\eta$.

Each interaction block updates a center feature by attending from the sample-point representation to its neighbour features. The attention scores include a learnable distance bias with a locality prior, and the value features are modulated by an orientation gate. The main experiments use 3 interaction blocks, 4 attention heads, hidden dimension 128, and dropout rate 0.1.

The bandwidth head outputs $d(d+1)/2 + 1$ scalars for each sample point. The first $d(d+1)/2$ values parameterize a raw lower-triangular matrix, while the final scalar is passed through a sigmoid gate to control the magnitude of strictly lower-triangular entries. Diagonal entries are clipped and exponentiated to ensure positivity, and strictly lower-triangular entries are scaled by a conservative off-diagonal factor. The resulting lower-triangular factor L_i defines

$$H_i = L_i L_i^\top. \quad (\text{A5})$$

This Cholesky-type parameterization ensures that each predicted bandwidth matrix is symmetric positive definite. The full-matrix form allows locally anisotropic smoothing, while the SPD constraint ensures that the resulting Gaussian kernels are valid density kernels.

For numerical stability, density evaluation is performed using log-domain summation, and matrix solves are implemented through triangular operations associated with the Cholesky factors rather than explicit matrix inversion. Dimension-dependent numerical defaults are used for diagonal clipping, off-diagonal scaling, and optional shrinkage.

C Implementation Details of Baseline Methods

This section describes the baseline methods, NNKDE variants, and numerical implementation details used in the experiments.

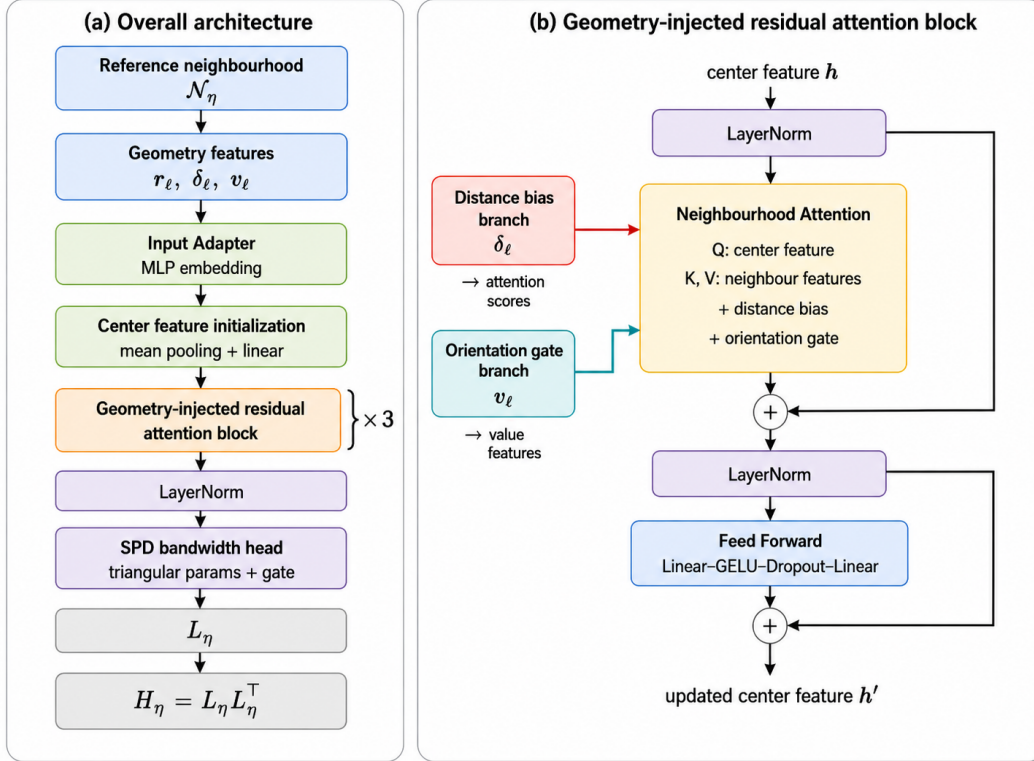


Fig. A1: Architecture of the neural bandwidth recommender $\phi_\theta : \mathcal{N}_\eta \rightarrow H_\eta$ for a generic reference location $\eta \in \mathbb{R}^d$.

Scott and Silverman rules (Scott / Silverman). Scott’s and Silverman’s rules are normal-reference bandwidth selectors for KDE [Scott, 1992, Silverman, 1986]. They use a single global bandwidth determined from the sample size, dimension, and empirical scale of the data. These methods are included as simple rule-of-thumb KDE baselines.

Global KDE with likelihood cross-validation (LCV). The global KDE-LCV baseline uses a single global bandwidth selected by likelihood cross-validation [Rudemo, 1982, Bowman, 1984]. This baseline optimizes the smoothing scale using the observed sample, but it still applies one global bandwidth structure to the entire dataset.

Abramson adaptive KDE (Abramson). The Abramson baseline is a classical adaptive KDE method based on local bandwidth rescaling [Abramson, 1982, Terrell and Scott, 1992]. It adjusts the local bandwidth magnitude according to a pilot density estimate. This provides a non-neural sample-point adaptive KDE baseline.

kNN local-scaling KDE (kNN). The kNN local-scaling baseline assigns local bandwidth scales using nearest-neighbour distances. It is included as a simple geometry-based adaptive KDE method, related to nearest-neighbour density estimation and sample-point adaptive smoothing [Loftsgaarden and Quesenberry, 1965, Breiman et al., 1977].

D Scenarios for Method Comparison

Scenarios $\text{GMD}_{\mathcal{F}}$ and $\text{GMD}_{\mathcal{F}+}$. The generation rule of the target distribution F_0 in scenario $\text{GMD}_{\mathcal{F}}$ has been explicitly established in Appendix A. In scenario $\text{GMD}_{\mathcal{F}+}$, we keep the same setting except that the eigenvalue distribution of Σ_k is changed from $\text{Unif}([0.25, 2.50])$ to

$\text{Unif}([0.15, 0.25])$. This modification leads to more compact Gaussian components than in the $\text{GMD}_{\mathcal{F}}$ scenario.

Scenario Banana. In this scenario, we generate the target distribution F_0 from the *Banana-shaped family*, a nonlinear non-Gaussian distribution family parameterized by a curvature parameter b and coordinate-wise noise standard deviations $\sigma_{1:d}$. Specifically, for each sample $X_i = (X_{i,1}, \dots, X_{i,d}) \in \mathbb{R}^d$, the coordinates are generated autoregressively as follows:

$$X_{i,1} \sim N(0, \sigma_1^2), \quad X_{i,k} | X_{i,k-1} \sim N(b(X_{i,k-1}^2 - \sigma_{k-1}^2), \sigma_k^2), \quad k = 2, \dots, d. \quad (\text{A6})$$

This construction creates nonlinear dependence across coordinates through the quadratic drift term while retaining a tractable density by the autoregressive factorization

$$f_0(x_i) = f_1(x_{i,1}) \prod_{k=2}^d f_k(x_{i,k} | x_{i,k-1}). \quad (\text{A7})$$

In the experiment, we sample $b \sim \text{Unif}[0.08, 0.35]$ and independently sample $\sigma_k \sim \text{Unif}[0.05, 0.30]$ for $k = 1, \dots, d$.

Scenario Noisy Torus. In this scenario, we generate the target distribution F_0 from a *noisy torus-type family*, whose probability mass concentrates near a low-dimensional circular manifold embedded in \mathbb{R}^d . The construction uses one noisy circular block when $d = 2$ or 3 , and two independent noisy circular blocks when $d \geq 4$. Let $k_d = 1$ for $d < 4$ and $k_d = 2$ for $d \geq 4$, and let $r_d = d - 2k_d$ be the number of remaining Gaussian noise coordinates.

For $j = 1, \dots, k_d$, generate

$$Z_j = (R_j + \sigma_r \rho_j)(\cos \theta_j, \sin \theta_j)^\top, \quad \theta_j \sim \text{Unif}(0, 2\pi), \quad \rho_j \sim N(0, 1). \quad (\text{A8})$$

If $r_d > 0$, generate $E \sim N(0, I_{r_d})$ and set $Y = (Z_1^\top, \dots, Z_{k_d}^\top, \sigma_\perp E^\top)^\top$; otherwise set $Y = (Z_1^\top, \dots, Z_{k_d}^\top)^\top$. The final observation is

$$X = \mu + QY, \quad (\text{A9})$$

where Q is a random orthogonal matrix and $\mu \sim \text{Unif}([-1, 1]^d)$.

The noise levels are sampled as $\sigma_r \sim \text{Unif}([0.03, 0.06])$ and $\sigma_\perp \sim \text{Unif}([0.004, 0.012])$. When $k_d = 1$, the radius is sampled as $R_1 \sim \text{Unif}([2.0, 3.2])$. When $k_d = 2$, we sample $R_{\text{out}} \sim \text{Unif}([2.0, 3.2])$ and $\Delta_R \sim \text{Unif}([1.0, 1.8])$, and set

$$R_1 = R_{\text{out}}, \quad R_2 = \max\{R_{\text{out}} - \Delta_R, 0.25\}. \quad (\text{A10})$$

Thus $d = 2$ gives one noisy circle, $d = 3$ gives one noisy circle with one Gaussian coordinate, $d = 4$ gives a noisy product of two circles, and $d > 4$ adds $d - 4$ Gaussian coordinates.

All target families used in these four scenarios have tractable oracle log densities and scores, which allows a convenient evaluation pipeline for comparing methods.

E Additional Results

Table A1 provides additional comparison of different methods in the cross-section of $n = 4, 096$ with more numerical details. Each cell in the table reports two numbers for an experimental setting: the average NLL and the corresponding standard deviation. In general, the table delivers similar messages as in Figure 3. An interesting discovery from this table is that the NNKDE methods tend to enjoy a smaller performance variation than the other methods in most high-dimensional cases.

Table A1: Additional comparison of different methods in the cross-section of $n = 4096$

Gaussian mixture distributions from the pre-training family \mathcal{F} (scenario GMD $_{\mathcal{F}}$)							
Method	$d = 2$	$d = 3$	$d = 5$	$d = 10$	$d = 20$	$d = 30$	$d = 50$
Silverman	2.166 (0.167)	2.137 (0.213)	1.872 (0.311)	1.944 (0.228)	1.978 (0.256)	2.050 (0.292)	2.211 (0.237)
LCV	2.079 (0.126)	1.995 (0.174)	1.710 (0.199)	1.694 (0.120)	1.717 (0.104)	1.734 (0.127)	1.830 (0.067)
kNN	2.086 (0.121)	2.058 (0.191)	1.881 (0.212)	2.211 (0.134)	2.599 (0.079)	2.831 (0.093)	3.167 (0.027)
Abramson	2.088 (0.130)	1.999 (0.175)	1.714 (0.193)	1.719 (0.096)	1.717 (0.104)	1.734 (0.127)	1.830 (0.067)
NNKDE _{scratch}	2.149 (0.114)	2.072 (0.159)	1.790 (0.142)	1.689 (0.074)	1.672 (0.050)	1.678 (0.064)	1.784 (0.047)
NNKDE _{pre}	<u>2.068 (0.118)</u>	1.973 (0.165)	1.664 (0.167)	1.621 (0.089)	1.599 (0.052)	1.611 (0.061)	<u>1.687 (0.033)</u>
NNKDE _{fine}	2.067 (0.118)	<u>1.978 (0.166)</u>	<u>1.670 (0.170)</u>	<u>1.624 (0.090)</u>	<u>1.605 (0.052)</u>	<u>1.612 (0.062)</u>	1.685 (0.032)
Oracle	2.056 (0.117)	1.954 (0.162)	1.640 (0.165)	1.580 (0.086)	1.545 (0.052)	1.515 (0.057)	1.538 (0.040)
Gaussian mixture distributions out of the pre-training family \mathcal{F} (scenario GMD $_{\mathcal{F}+}$)							
Method	$d = 2$	$d = 3$	$d = 5$	$d = 10$	$d = 20$	$d = 30$	$d = 50$
Silverman	1.729 (0.266)	1.237 (0.448)	1.328 (0.466)	1.645 (0.409)	1.928 (0.397)	2.040 (0.340)	2.149 (0.186)
LCV	1.370 (0.226)	1.009 (0.271)	0.983 (0.246)	1.146 (0.252)	1.355 (0.244)	1.429 (0.274)	1.511 (0.165)
kNN	<u>1.245 (0.205)</u>	0.970 (0.215)	0.984 (0.175)	1.310 (0.112)	1.729 (0.068)	1.940 (0.053)	2.231 (0.028)
Abramson	1.385 (0.228)	1.026 (0.285)	1.008 (0.251)	1.159 (0.230)	1.365 (0.217)	1.429 (0.274)	1.511 (0.165)
NNKDE _{scratch}	1.700 (0.182)	1.437 (0.168)	1.341 (0.113)	1.189 (0.052)	1.107 (0.024)	1.166 (0.017)	1.124 (0.007)
NNKDE _{pre}	1.249 (0.200)	<u>0.947 (0.196)</u>	<u>0.799 (0.117)</u>	<u>0.845 (0.048)</u>	<u>0.802 (0.027)</u>	<u>0.866 (0.019)</u>	<u>0.981 (0.008)</u>
NNKDE _{fine}	1.234 (0.195)	0.918 (0.188)	0.794 (0.116)	0.768 (0.060)	0.746 (0.030)	0.765 (0.028)	0.789 (0.011)
Oracle	1.210 (0.194)	0.903 (0.184)	0.764 (0.110)	0.706 (0.054)	0.664 (0.029)	0.643 (0.019)	0.632 (0.008)
Banana-shaped distributions (scenario Banana)							
Method	$d = 2$	$d = 3$	$d = 5$	$d = 10$	$d = 20$	$d = 30$	$d = 50$
Silverman	-0.428 (0.326)	-0.536 (0.293)	<u>-0.437 (0.179)</u>	-0.364 (0.133)	<u>-0.265 (0.103)</u>	-0.200 (0.067)	-0.138 (0.049)
LCV	-0.429 (0.327)	<u>-0.537 (0.293)</u>	-0.438 (0.179)	<u>-0.371 (0.132)</u>	-0.282 (0.101)	<u>-0.227 (0.066)</u>	<u>-0.181 (0.048)</u>
kNN	-0.422 (0.326)	-0.503 (0.288)	-0.271 (0.170)	0.127 (0.128)	0.620 (0.096)	0.907 (0.063)	1.232 (0.047)
Abramson	-0.424 (0.328)	-0.530 (0.294)	-0.421 (0.179)	-0.235 (0.130)	-0.121 (0.098)	-0.077 (0.065)	-0.043 (0.047)
NNKDE _{scratch}	0.977 (0.020)	1.023 (0.014)	1.059 (0.009)	0.945 (0.009)	0.883 (0.006)	0.995 (0.005)	0.955 (0.002)
NNKDE _{pre}	-0.162 (0.189)	-0.198 (0.154)	0.080 (0.046)	0.494 (0.027)	0.392 (0.013)	0.575 (0.009)	0.771 (0.004)
NNKDE _{fine}	-0.429 (0.329)	-0.538 (0.295)	-0.434 (0.182)	-0.399 (0.136)	-0.258 (0.084)	-0.295 (0.072)	-0.232 (0.054)
Oracle	-0.435 (0.328)	-0.549 (0.294)	-0.469 (0.179)	-0.449 (0.136)	-0.418 (0.104)	-0.403 (0.072)	-0.424 (0.057)
Noisy torus distributions (scenario NoisyTorus)							
Method	$d = 2$	$d = 3$	$d = 5$	$d = 10$	$d = 20$	$d = 30$	$d = 50$
Silverman	1.437 (0.090)	1.004 (0.109)	1.047 (0.121)	0.564 (0.215)	0.185 (0.157)	0.006 (0.160)	-0.179 (0.211)
LCV	1.107 (0.087)	0.553 (0.105)	<u>0.650 (0.116)</u>	<u>0.022 (0.210)</u>	<u>-0.431 (0.154)</u>	-0.634 (0.159)	-0.838 (0.208)
kNN	0.897 (0.081)	<u>0.302 (0.087)</u>	1.345 (0.135)	1.009 (0.254)	0.734 (0.245)	0.681 (0.193)	0.623 (0.285)
Abramson	1.107 (0.087)	0.554 (0.105)	0.654 (0.116)	0.026 (0.212)	-0.430 (0.157)	<u>-0.637 (0.160)</u>	<u>-0.854 (0.213)</u>
NNKDE _{scratch}	1.844 (0.048)	1.594 (0.044)	1.555 (0.059)	1.201 (0.057)	0.988 (0.026)	1.049 (0.014)	0.974 (0.013)
NNKDE _{pre}	1.294 (0.056)	0.743 (0.061)	0.957 (0.052)	0.794 (0.048)	0.500 (0.035)	0.657 (0.011)	0.841 (0.003)
NNKDE _{fine}	<u>1.022 (0.074)</u>	0.064 (0.103)	0.440 (0.191)	-0.591 (0.223)	-1.020 (0.051)	-1.231 (0.076)	-1.014 (0.076)
Oracle	0.498 (0.118)	-0.837 (0.119)	-0.387 (0.064)	-1.907 (0.233)	-2.788 (0.192)	-3.026 (0.216)	-3.178 (0.250)